

Photonic Generation of Linear-Frequency-Modulated Waveforms With Improved Time-Bandwidth Product Based on Polarization Modulation

Yamei Zhang, *Student Member, IEEE*, Xingwei Ye, *Student Member, IEEE*, Qingshui Guo, Fangzheng Zhang, and Shilong Pan, *Senior Member, IEEE*

Abstract—Polarization modulation of two phase-correlated, orthogonally polarized wavelengths by a parabolic waveform is a promising way to generate linear-frequency-modulated (LFM) signals, but the time-bandwidth product (TBWP) of the generated LFM signal is intrinsically limited by the achievable modulation index of the polarization modulator (PolM). In this paper, an approach to increase the TBWP of the LFM signal generated by polarization modulation is proposed and comprehensively studied by splitting the electrical parabolic waveforms into N pieces with identical amplitude. Applying the split parabolic signal to the PolM, the total equivalent phase shift would be boosted by $N/2$ times. As a result, the bandwidth as well as the TBWP of the generated LFM signal is increased by $N/2$ times. An experiment is carried out. As compared to the scheme using an unsplit parabolic signal, the TBWP is improved by more than 500 times. The relationships between the bandwidth, the time duration, and the TBWP of the generated signal with the parameters of the electrical waveform generator are discussed.

Index Terms—Linear frequency modulation, microwave photonics, pulse compression, time-bandwidth product.

I. INTRODUCTION

LINEAR frequency-modulated (LFM) waveforms are widely used in radar systems to achieve simultaneous large detection range and high range resolution thanks to their pulse compression capability [1], [2]. With the fast development of millimeter-wave and terahertz-wave technologies, LFM signals with a central frequency of up to tens or even hundreds of gigahertz and an instantaneous bandwidth of a few gigahertz are often desired. Conventionally, LFM waveforms are generated

Manuscript received July 21, 2016; revised December 3, 2016; accepted December 27, 2016. Date of publication January 10, 2017; date of current version April 20, 2017. This work was supported in part by the National Natural Science Foundation of China under Grant 61422108, Grant 61401201, and Grant 61527820, in part by the Funding for Outstanding Doctoral Dissertation in Nanjing University of Aeronautics and Astronautics under Grant BCXJ15-02, in part by the Funding of Jiangsu Innovation Program for Graduate Education (KYLX15_0280), and in part by the Fundamental Research Funds for the Central Universities.

The authors are with the Key Laboratory of Radar Imaging and Microwave Photonics and the Ministry of Education, Nanjing University of Aeronautics and Astronautics, Nanjing 210016, China (e-mail: zhang_ym@nuaa.edu.cn; yexw@nuaa.edu.cn; zczkgqs@126.com; zhangfangzheng@nuaa.edu.cn; pans@iee.org).

Color versions of one or more of the figures in this paper are available online at <http://ieeexplore.ieee.org>.

Digital Object Identifier 10.1109/JLT.2017.2651902

using electrical circuits. However, because of the well-known electronic bottleneck, direct generation of the LFM signal in the electrical domain would suffer from limited instantaneous bandwidth, low central frequency and complicated configurations. To deal with these problems, photonic technologies for LFM signal generation have been reported [3]–[20] because photonic technologies can provide distinct features in terms of broad bandwidth, low loss and immunity to electromagnetic interference. Many methods have been proposed in the past few years to generate the LFM signals using photonic technologies, which can be generally divided into two categories. One is based on pulse shaping, either direct space-to-time (DST) pulse shaping [3]–[4] or spectral shaping together with frequency-to-time mapping (FTTM) [5]–[10], and the other is based on external phase modulation followed by optical heterodyning [11]–[22].

DST pulse shaping is implemented by shaping the envelope of input optical pulses in the time domain with free-space components [3] or arrayed waveguide gratings [4]. When these pulses are introduced to a bandwidth-limited photodetector (PD), the envelope would be detected, which forms an electrical LFM waveform. LFM waveform generation based on spectral shaping and FTTM is to manipulate the spectrum of the input optical pulse to have a shape of the scaled version of an LFM waveform. When this signal is propagating through a dispersive element, the spectral shape is mapped into the time domain, generating an LFM waveform. Both of these methods can generate LFM waveforms with an instantaneous bandwidth up to tens of gigahertz, but the time durations are usually limited to a few hundreds of picoseconds or several nanoseconds, resulting in a very small time-bandwidth product (TBWP) (around 100).

To improve the TBWP, an optical interferometric configuration can be employed [9], but it is very difficult to eliminate the phase jitter introduced by the optical path separation. In addition, the maximal TBWP is limited by the total number of the resolution element of the pulse shaper, which is generally smaller than 500. Recently, A. M. Weiner *et al.* proposed a method to improve the TBWP by phase coding the generated LFM waveform with a pseudo-random sequence [10]. With the phase coding, the effective duration of the LFM waveform can be increased by thousands of times while keeping the instantaneous bandwidth unchanged, so the TBWP can be improved to be larger than 80,000. However, with phase coding, the

synthesized LFM signal would be sensitive to Doppler shift, which would reduce the range resolution when the signal is employed in a radar system.

LFM waveforms can also be generated by introducing a parabolic phase difference to two phase-correlated optical wavelengths followed by optical heterodyning in a PD. The phase difference can be introduced by a phase modulator (PM) [11]–[13], but the two phase-correlated optical wavelengths have to be spatially separated to ensure that only one wavelength undergoes the phase modulation, which would inevitably introduce serious phase jitter to the generated signals [11]–[12]. To avoid the optical path separation, a polarization modulator (PoIM), which can introduce two opposite phase modulations to two orthogonal polarization directions, is employed [14]–[16].

The key of the proposed method is to generate two orthogonally-polarized and phase-correlated optical wavelengths. Previously, the two wavelengths were generated based on a differential group delay (DGD) [15]–[16], stimulated Brillouin scattering (SBS) induced polarization rotation [17], or external polarization modulation [18]–[21]. The key limitation associated with the external-phase-modulation based method is the small TBWP of the generated LFM signal, which is restricted by the maximum achievable modulation index of the electro-optical modulator (generally smaller than 10). To enlarge the TBWP of the generated LFM waveform, a recirculating phase modulation loop (RPML) can be employed [22]. By recirculating one optical wavelength in the RPML and introducing a parabolic phase modulation during each recirculation, an LFM signal with the TBWP increased by 16 times is generated. However, the circulation times are limited to about 20 due to the insertion loss of the devices used in the loop. In addition, the larger the duty cycle is, the smaller the recirculating time will be.

Recently, we have proposed a photonic approach to generate LFM waveforms with an improved TBWP by splitting the electrical parabolic driving signal into N pieces [23]. However, only a proof-of-concept experiment was conducted, which did not provide any detailed analysis of the capability and limitation of the method for improving the TBWPs of the generated LFM waveforms. In addition, LFM waveforms with TBWP improved by only 50 times were generated, which is still too small to meet practical requirements.

In this paper, a comprehensive study of the PoIM-based LFM signal generator with a split electrical parabolic driving signal is performed. In the system, two orthogonally-polarized phase-correlated wavelengths are first generated. Then, a PoIM driven by a parabolic signal is employed to introduce a parabolic phase difference to the two wavelengths. With a polarizer to combine the two orthogonally-polarized wavelengths and a PD to convert the optical signal into the electrical domain, an LFM waveform is generated. Splitting the parabolic waveform into N pieces with identical amplitude while maintaining the total time duration unchanged, the effective modulation index of the PoIM would be increased by $N/2$ times (N is the number of the split pieces), so will be the bandwidth and the TBWP of the generated LFM signal. However, the larger N is, the higher the sampling rate of the electrical waveform generator will be required.

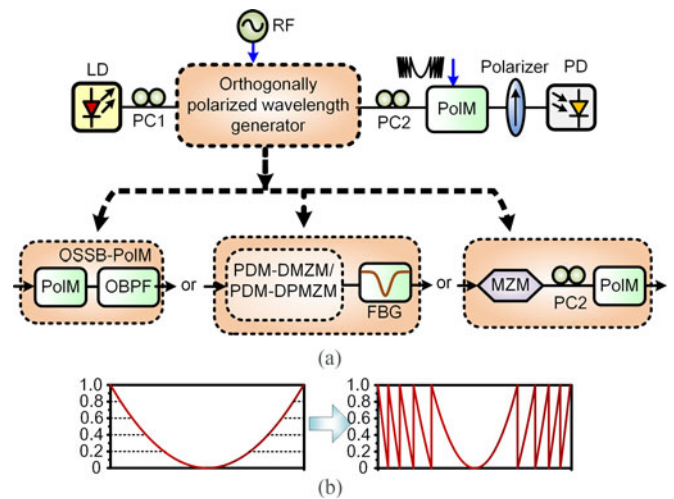


Fig. 1. (a) Schematic diagram of the proposed photonic LFM waveform generator. LD: laser diode; PC: polarization controller; OBPF: optical bandpass filter; MZM: Mach-Zehnder modulator; PDM-DMZM: polarization division multiplexing dual-arm MZM; PDM-DPMZM: PDM dual-parallel MZM; FBG: fiber Bragg grating; PoIM: polarization modulator; OSSB-PoIM: optical single-sideband PoIM; PD: photodetector. (b) Schematic of the conventional parabolic signal (left) and the split parabolic signal (right) when the split number is equal to 10.

To lower the performance requirements of the electrical waveform generator, the parabolic signals can be first time-stretched by $N/2$ times, split into N pieces, and amplified to the maximum achievable magnitude. As compared with the case with an unsplit parabolic driving signal, the bandwidth of the generated LFM waveform remains almost unchanged while the TBWP is improved by $N/2$ times. An experiment is carried out to verify the feasibility of the proposed scheme. The generation of LFM waveforms with a TBWP increased by more than 500 times is experimentally demonstrated as compared with the case using an unsplit parabolic driving signal. The distortions induced by the non-ideal electrical driving waveforms and imperfect orthogonal polarization states are analyzed. The relationships between the bandwidth, the time duration and the TBWP of the generated LFM waveforms with the parameters of the electrical waveform generator, such as, the sampling rate, memory depth, etc. are discussed. The method can possibly be applied together with the RPML [22] to generate LFM waveforms with TBWPs of more than 10,000.

II. PRINCIPLE

Fig. 1(a) shows the schematic diagram of the proposed photonic LFM waveform generator, which consists of a laser diode (LD), an orthogonally-polarized-wavelength generator, a PoIM, a polarization controller (PC), a polarizer and a PD. The orthogonally-polarized-wavelength generator can be implemented based on an optical single-sideband PoIM (OSSB-PoIM) [18], a Mach-Zehnder modulator (MZM) incorporated with a PoIM [20], a polarization-division multiplexing (PDM) dual-arm MZM (PDM-DMZM), or a PDM dual-parallel MZM (PDM-DPMZM) [21], [24]. The schematic diagrams of the three types of orthogonally-polarized-wavelength generators are

shown in the insets of Fig. 1(a). With different experimental setups, orthogonally-polarized wavelengths separated by one time, two times, four times or eight times of the frequency of the electrical driving RF signal can be generated, respectively. As a result, LFM signals with a central frequency far beyond the operation frequency range of the electrical and optoelectronic devices can be generated.

Among the orthogonally-polarized-wavelength generators listed in Fig. 1(a), the OSSB-PoIM is the simplest one, which is therefore applied in this work to study the TBWP improvement by the split electrical parabolic driving signal. Continuous-wave light from the LD is fed into the OSSB-PoIM. A PC (PC1) is inserted before the OSSB-PoIM to let the angle between the polarization direction of the input light and one of the principal axes of the OSSB-PoIM be 45° . After the OSSB-PoIM, another PC (PC2) is employed to rotate the state of the polarization of the OSSB polarization-modulated signal by 45° . Suppose the expression of the optical carrier is $E_o = \cos(j\omega_o t)$, and that of the RF driving signal is $E_m = \cos(\omega_m t)$, where ω_o and ω_m are the angular frequencies of the optical carrier and the RF signal, respectively, the signal at the output of PC2 consists of two orthogonally-polarized phase-correlated wavelengths [18], i.e.

$$E_{PC2} = \begin{bmatrix} A_1 \cos(\omega_o t + \phi_0) \\ A_2 \cos(\omega_o t - \omega_m t) \end{bmatrix} \quad (1)$$

where A_1 and A_2 are the parameters related to the modulation index of the OSSB-PoIM [18], and ϕ_0 is the initial phase difference between the two polarization directions. Then, the two optical carriers are coupled into the second PolM (PolM2), in which the principal axes are aligned with those of the OSSB-PoIM. Assuming the expression of the driving signal introduced to PolM2 is $s(t)$, the optical field at the output of the PolM can be written as

$$E_{PoIM} \propto \begin{bmatrix} A_1 \cos\left(\omega_o t + \phi_0 + \gamma_s \frac{s(t)}{V_s}\right) \\ A_2 \cos\left(\omega_o t + \omega_m t + \gamma_s \frac{s(t)}{V_s}\right) \end{bmatrix} \quad (2)$$

where γ_s is the modulation index of PolM2, and V_s is the peak amplitude of $s(t)$. As can be seen from (2), complementary phase modulations are introduced to the two orthogonally-polarized wavelengths. With a polarizer to combine the two wavelengths, we have

$$E_{pol} \propto \frac{1}{\sqrt{2}} \left[A_1 \cos\left(\omega_o t + \phi_0 + \gamma_s \frac{s(t)}{V_s}\right) + A_2 \cos\left(\omega_o t + \omega_m t + \gamma_s \frac{s(t)}{V_s}\right) \right] \quad (3)$$

Then, the combined optical signals are sent to a PD, and the AC term of the photocurrent is

$$I_{AC}(t) \propto \frac{A_1 A_2}{2} \cos\left(\omega_m t + \phi_0 + 2\gamma_s \frac{s(t)}{V_s}\right) \quad (4)$$

As a result, a phase-modulated microwave signal with an angular frequency of ω_m and a phase term of $\phi_0 + 2\gamma_s s(t) / V_s$ is generated. When $s(t)$ is a parabolic signal as the left figure of

Fig. 1(b) shows, i.e.

$$s(t) = V_s \begin{cases} K(t - T_0/2)^2, & 0 \leq t \leq T_0 \\ 0, & \text{else} \end{cases} \quad (5)$$

where K is a constant equal to $4/T_0^2$, (4) can be rewritten as

$$I_{AC}(t) \propto \begin{cases} \frac{A_1 A_2}{2} \cos\left[\omega_m t + \phi_0 + 2\gamma_s K(t - T_0/2)^2\right], & 0 \leq t \leq T_0 \\ \frac{A_1 A_2}{2} \cos(\omega_m t + \phi_0), & \text{else} \end{cases} \quad (6)$$

The instantaneous frequency of the generated signal in (6) is the derivation of the phase term, which is

$$\omega_I = \begin{cases} \omega_m + 4\gamma_s K(t - T_0/2), & 0 \leq t \leq T_0 \\ \omega_m, & \text{else} \end{cases} \quad (7)$$

Therefore, the generated signal is an LFM signal as the instantaneous frequency changes linearly according to the time value “ t ”. And the bandwidth of the generated LFM signal is

$$B_f = \frac{4\gamma_s K T_0}{2\pi} = \frac{8\gamma_s}{\pi T_0} \quad (8)$$

so the TBWP of the generated LFM signal is given by

$$TBWP = B_f * T_0 = \frac{8\gamma_s}{\pi} \quad (9)$$

As can be seen from (9), the TBWP of the generated LFM waveform depends only on the modulation index of PolM2, which is determined by

$$\gamma_s = \pi V_s / 2V_\pi \quad (10)$$

where V_π is the half-wave voltage of PolM2. To improve the TBWP, one has to enlarge the modulation index, which can be realized by increasing the input power of the parabolic signal or by decreasing the half-wave voltage of PolM2. Considering the modulator after fabrication has a fixed half-wave voltage, the feasible way to improve the TBWP is to increase the input power. However, the maximum allowable electrical power to the PolM is generally limited to less than 1 W, indicating that the TBWP of the LFM signal generated with the parabolic signal is limited, typically to less than 10.

To solve this problem, we propose in this work to split the parabolic signal into N pieces, which are amplified to the same peak amplitude as large as that the modulator can tolerate. The split signal can be expressed as

$$s(t) = \frac{N}{2} V_s \begin{cases} K(t - T_0/2)^2 + C_1, & 0 \leq t < t_1 \\ K(t - T_0/2)^2 + C_2, & t_1 \leq t < t_2 \\ \dots & \dots \\ K(t - T_0/2)^2 + C_N, & t_{N-1} \leq t \leq T_0 \\ 0, & \text{else} \end{cases} \quad (11)$$

where C_n ($n = 1, 2, \dots, N$) is a constant to adjust the signal in each piece to have the same peak amplitude. When $N = 10$,

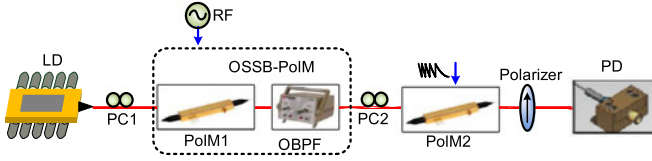


Fig. 2. Experimental setup of the proposed LFM generator.

the split parabolic signal has a shape like the right figure of Fig. 1(b). Because the instantaneous frequency of the generated LFM signal is proportional to the differential of $s(t)$, the values of C_n have no impacts on the instantaneous frequency. Using this signal as the driving signal to PolM2, the bandwidth of the generated signal becomes

$$B_f' = \frac{N4\gamma_s KT_0}{4\pi} = \frac{4N\gamma_s}{\pi T_0} \quad (12)$$

As can be seen, the bandwidth of the generated LFM signal is related to the parameters of N , γ_s and T_0 . If the modulation index of the proposed system is fixed, the bandwidth of the generated LFM signal is proportional to N/T_0 . If the time duration T_0 is also fixed, the bandwidth would be increased by $N/2$ times when the parabolic signal is split into N pieces, and the TBWP can be improved by $N/2$ times. If the bandwidth of the generated LFM signal is required to be constant while the TBWP needs to be increased, one can stretch the parabolic signal in the time domain, and then select an N to let N/T_0 be a constant.

Substituting (12) into (9), the TBWP is increased to

$$TBWP' = B_f' * T_0 = \frac{4N\gamma_s}{\pi} \quad (13)$$

Therefore, the TBWP can be improved by $N/2$ times when a split parabolic signal with a split number of N is applied to the proposed LFM system. It should be noted that the proposed approach can work together with the RPML-based method [22], to further improve the TBWP.

III. EXPERIMENTS AND RESULTS

An experiment is carried out based on the experimental setup in Fig. 2. The wavelength and the output power of the LD are 1,552.442 nm and 16 dBm, respectively. The 3-dB bandwidth and the half-wave voltage of the PolMs are 40 GHz and 3.5 V, respectively. The microwave signal generated by a signal generator (Agilent 8257D) has a power of 15 dBm. By applying the microwave signal to the OSSB-PoIM, which consists of a PolM (PolM1) and an optical bandpass filter (OBPF), an OSSB polarization-modulated signal is generated. This signal is fed into another PolM (PolM2) which is driven by a parabolic signal generated by an arbitrary waveform generator (AWG, Keysight M8195A) with a sampling rate of 65 GSa/s. After a polarizer, the OSSB polarization-modulated signal is fed into a PD with a 3-dB bandwidth of 50 GHz and a responsivity of 0.65 A/W. The electrical waveforms are observed by an 80 GSa/s real-time oscilloscope (Agilent DSO-X 92504A) and the optical spectra are measured by an optical spectrum analyzer with a resolution of 0.02 nm (AQ6370C).

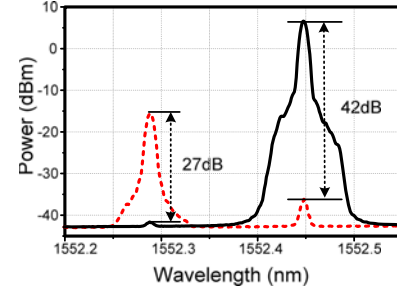


Fig. 3. The optical spectra of the orthogonally-polarized optical wavelengths.

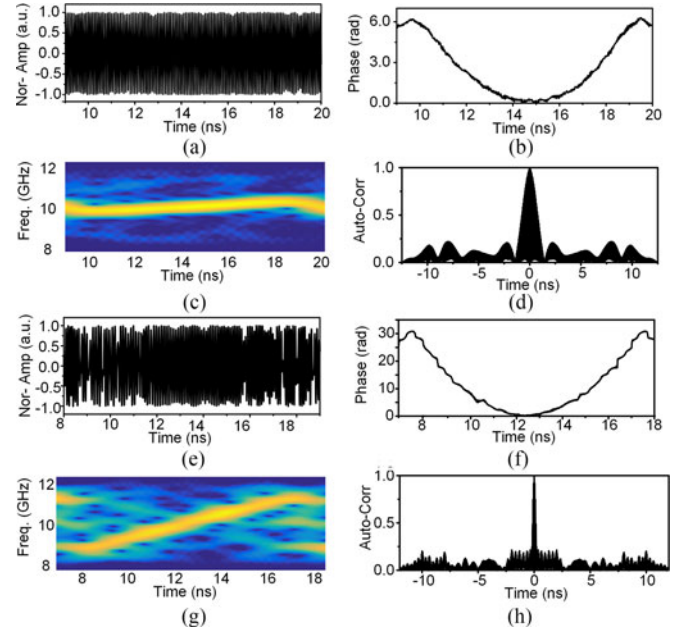


Fig. 4. The experimental results for the LFM generation (a)–(d) using an unsplit parabolic signal, and (e)–(h) using a split parabolic signal with a split number $N = 10$. (a), (e) The generated LFM waveforms, (b), (f) the recovered phases, (c), (g) the instantaneous frequencies, and (d), (h) the auto-correlation functions.

Fig. 3 shows the optical spectra observed at the output of the OSSB-PoIM based orthogonally-polarized-wavelength generator when a PC and a polarization beam splitter (PBS) are connected. As can be seen, in each polarization direction, only one optical wavelength is observed while the other is more than 27 dB lower, indicating that the two wavelengths at the output of PC2 are indeed orthogonally polarized.

The two orthogonally-polarized optical wavelengths are sent directly to the optical port of PolM2 which is driven by an unsplit parabolic waveform with a peak voltage of 7 V. The duration of the parabolic pulse is 10 ns. Fig. 4(a) shows the waveform of the LFM signal, and its phase is shown in Fig. 4(b) which is extracted by Hilbert transformation of the waveform in Fig. 4(a). A phase curve with a parabolic shape is observed. Fig. 4(c) shows the instantaneous frequency of the LFM waveform obtained by short-time Fourier transform. The bandwidth of the LFM signal is about 740 MHz. As the time duration is 10 ns, the TBWP of the generated LFM signal is 7.4. Fig. 4(d) shows the auto-correlation function of the

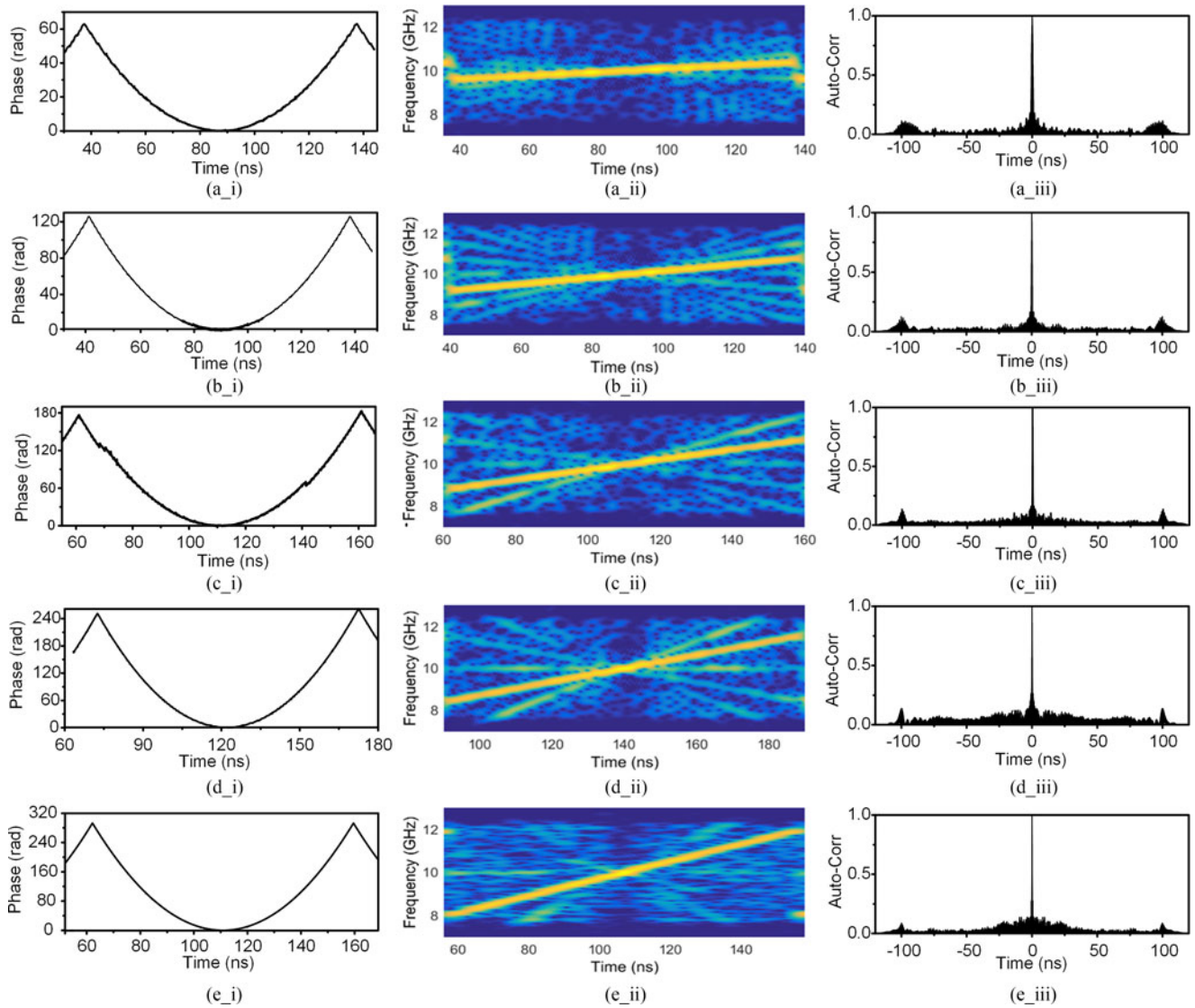


Fig. 5. The phases, instantaneous frequencies and auto-correlation functions of the generated LFM signals with different splitnumbers when $T_0 = 100$ ns. (a) $N = 20$, (b) $N = 40$, (c) $N = 60$, (d) $N = 80$ and (e) $N = 100$.

generated LFM waveform. The full-width at half maximum (FWHM) of the compressed pulse is about 1.39 ns, so the pulse compression ratio is 7.19. Because the pulse compression ratio after autocorrelation should be equal to the TBWP for LFM signals, the experiment confirms that LFM signal generation is realized.

Then, the parabolic signal is split into 10 pieces and applied to PolM2. Fig. 4(e) shows the waveform of the generated LFM signal. The amplitude variations might be introduced due to the imperfect photonic microwave phase modulation. Fig. 4(f) shows the recovered phase of the generated LFM signal, and Fig. 4(g) shows the instantaneous frequency, from which the bandwidth is calculated to be about 4.04 GHz. Thus, the TBWP is calculated to be 40.4. Fig. 4(h) shows the auto-correlation function. The FWHM of the compressed pulse is about 0.25 ns, corresponding to a pulse compression ratio of 40, which agrees well with the pulse compression ratio, indicating again that the generated signal is indeed a LFM signal. Compared with the

case using an unsplit parabolic driving signal, the bandwidth and TBWP of the LFM signal generated by the 10-piece split parabolic signal are improved by about 5 times, agreeing well with the theoretical prediction.

Then, parabolic signals with a fixed time duration of 100 ns and split numbers of 20, 40, 60, 80 and 100 are used to drive PolM2. The recovered phases, instantaneous frequencies as well as the auto-correlation functions of the generated LFM signal are shown in Fig. 5. As can be seen from Fig. 5(a)–(e), the maximum phase changes of the generated LFM signals are 62, 125, 180, 250 and 315 rad respectively, and the corresponding bandwidths are 0.76, 1.52, 2.24, 3.08 and 3.96 GHz. Both the maximum phase change ranges and the bandwidth of the generated LFM signals increase linearly according to the split number N . As the time duration is fixed to be 100 ns, the TBWP of the generated LFM signals are calculated to be 76, 152, 224, 308 and 396, respectively. The FWHM of the five compressed pulses after auto-correlation are 1.30 ns, 0.61 ns, 0.43 ns, 0.32 ns and 0.26 ns,

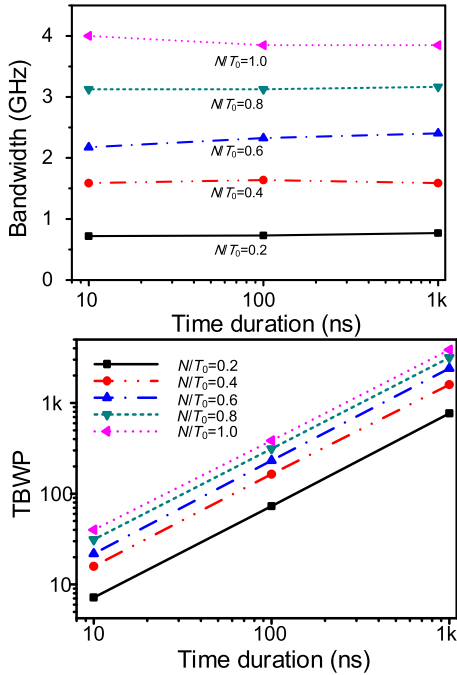


Fig. 6. (a) Bandwidth and (b) TBWP as a function of T_0 when N/T_0 is fixed.

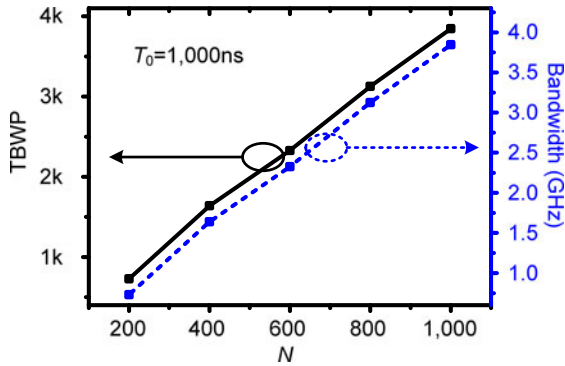


Fig. 7. TBWP and bandwidth as a function of split number N when T_0 is fixed to be 1,000 ns.

corresponding to pulse compression ratios of 72.9, 163.9, 232.6, 312.5 and 384.6, respectively.

Fig. 6 shows the TBWP and bandwidth as a function of the time durations under different ratios of N/T_0 . As can be seen, when N/T_0 is fixed, the bandwidth remains almost unchanged while the TBWP increases linearly with the time duration, which agrees well with the results predicted by (12) and (13).

Fig. 7 shows the TBWP and bandwidth of the generated LFM signals as a function of split number N when the time duration of the driving signal T_0 is fixed to be 1,000 ns. As expected, both the TBWP and the bandwidth increase linearly with N .

The instantaneous frequency and the auto-correlation function when N/T_0 is 1.0 ns⁻¹ and T_0 is 1,000 ns are shown in Fig. 8. The FWHM of the compressed pulse is calculated to be 0.26 ns, corresponding to a TBWP of about 3,846.2. Compared to the case using unsplit and unstretched parabolic driving

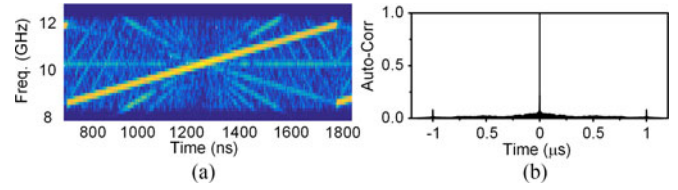


Fig. 8. (a) The instantaneous frequency and (b) the auto-correlation function of the generated LFM signal when a split parabolic driving signal with $T_0 = 1,000$ ns and $N = 1,000$ is employed.

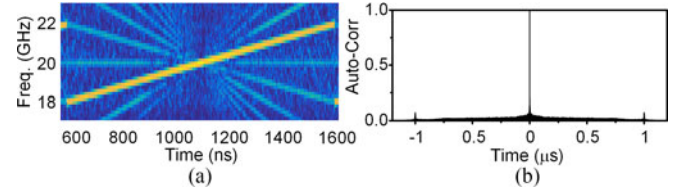


Fig. 9. (a) The instantaneous frequency and (b) the auto-correlation function of the generated signals with 20 GHz central frequency.

signal with a pulse width of 10 ns, the TBWP is improved by more than 500 times.

It should be noted that the proposed method can work with a RPML [22] to further increase the TBWP of the generated LFM waveform. Wideband LFM signals with very large TBWPs (e.g. more than 10,000) might be possibly generated.

IV. DISCUSSION

A. Tunability

For different applications, LFM waveforms with different central frequencies and different bandwidths will be required. In the proposed scheme, the bandwidth of the generated LFM signal can be tuned by controlling the ratio between the split number and the time duration of the driving parabolic signal, as can be seen in Figs. 6 and 7. The frequency tunability is implemented by adjusting the frequency of the RF signal to PolM1. The frequency tuning range is dependent on the orthogonally-polarized-wavelength generators. As explained in Section II, many schemes can be employed in the proposed LFM generation system, and different schemes have different frequency tuning ranges. For the OSSB-PolM based scheme used in the experiment, the frequency range depends mainly on the bandwidth of the electro-optical modulator and the optical filter, which is from 10 to 40 GHz [25]. If a frequency multiplication structure is employed [24], LFM signals with central frequencies up to hundreds of GHz can be generated.

To confirm the frequency tunability, a microwave signal centered at 20 GHz is applied to PolM1, and a parabolic signal with a split number of 1,000 and a time duration of 1,000 ns is applied to PolM2. The experimental result is shown in Fig. 9. As can be seen, the frequency range of the generated LFM signal is changed to 18–22 GHz, giving a bandwidth of about 4 GHz. The FWHM of the compressed pulse is about 0.246 ns, corresponding to a pulse compression ratio of about 4,065, which is very close to that of the 10-GHz case.

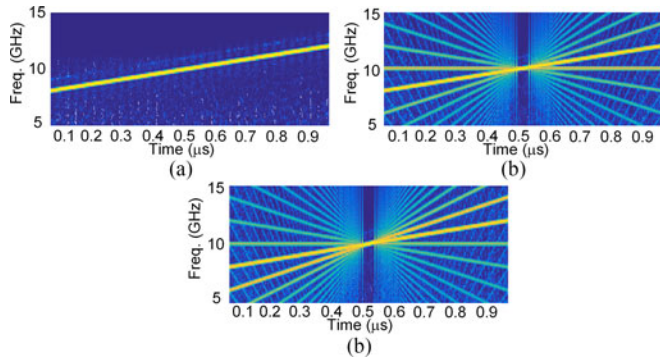


Fig. 10. The simulated instantaneous frequency diagrams of the generated LFM signals when split parabolic signals with (a) $C_n = 2\pi$, (b) $C_n < 2\pi$ and (c) $C_n > 2\pi$ are applied.

B. Undesirable Frequency Components

In Figs. 4, 5, 8, and 9, we can observe many several weak lines around the main lines in the instantaneous frequency diagrams. One factor to create these undesirable frequency components is the non-ideal split of the parabolic signal. From (11), the values of C_n should have no impacts on the instantaneous frequency since the instantaneous frequency is proportional to the differential of the phase. However, if $C_n \neq 2k\pi$ (k is an integer), a discontinuity point would be created in the phase curve and a lot of high-frequency components are therefore generated. Fig. 10 shows the simulated instantaneous frequency diagrams when split parabolic signals with $C_n = 2\pi$, $C_n < 2\pi$ and $C_n > 2\pi$ are applied to the PolM, respectively. Only one line can be observed when $C_n = 2\pi$, while many undesirable harmonic components are created when $C_n \neq 2\pi$. Ideally, one can carefully control the amplitude of the drive signal to let $C_n = 2\pi$. However, due to the uneven frequency response of the microwave devices and the electro-optical modulator, it is very difficult to achieve this ideal condition.

Another contributing factor of the undesirable frequency component generation is the non-ideal orthogonally-polarized-wavelength generator. If the two phase-correlated wavelengths generated by the orthogonally-polarized-wavelength generator are not orthogonal, the parabolic driving signal would affect the amplitude of the generated LFM signal, forming undesirable frequency components. To evaluate the orthogonality of the two phase-correlated wavelengths, we redefine polarization extinction ratio as the ratio of the total power of one wavelength and its power along the polarization direction of the other wavelength. Fig. 11 shows the simulated instantaneous frequency diagrams when the polarization extinction ratio is 20, 10 and 3 dB, respectively. As can be seen, the smaller the polarization extinction ratio is, the stronger the undesirable components will be.

In addition, the parabolic signal that is generated directly by the electrical waveform generator is also not ideal. A parabolic signal from the electrical waveform generator is recorded using an oscilloscope and then applied to the simulated system with all other components ideal. Fig. 12 shows the simulated instantaneous frequency diagram. As can be seen, there are many harmonic components.

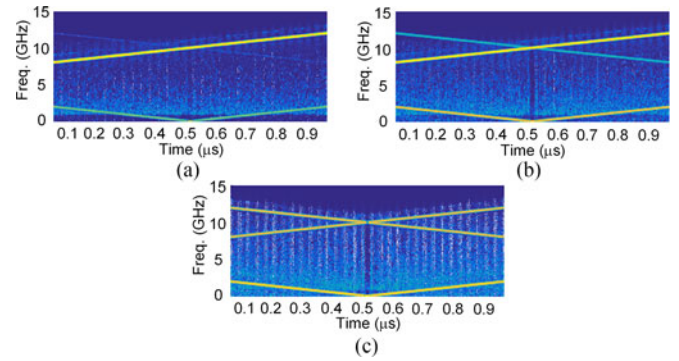


Fig. 11. The simulated instantaneous frequency diagrams of the generated signals with different polarization extinction ratio. (a) 20 dB, (b) 10 dB, and (c) 3 dB.

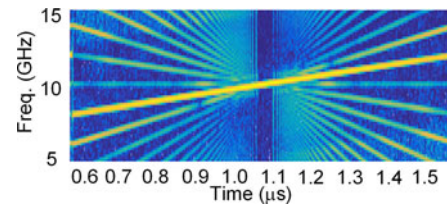


Fig. 12. The simulated instantaneous frequency diagram when a parabolic signal generated by the electrical waveform generator is applied to the simulated system.

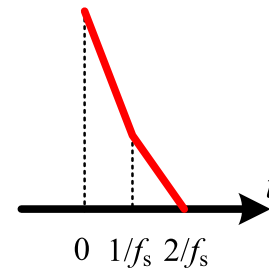


Fig. 13. The zoom in version of the first piece of the parabolic signal containing three points.

C. Limitations

Although the proposed method can significantly improve the TBWP or bandwidth of the generated LFM signal, the maximum achievable bandwidth, pulse width and TBWP are restricted by the sampling rate and the memory depth of the electrical waveform generator.

Supposing the maximum split number of the parabolic signal in (5) is N_m , and the sampling rate of electrical waveform generator is f_s , the maximum amplitude of each piece from the electrical waveform generator can be expressed as,

$$V_{Nm} = V_s \frac{K(0 - T_0/2)^2}{N_m/2} \quad (14)$$

To make the distortion of the generated signal acceptable, the first or last piece of the split parabolic signal, which has the largest slope in a parabolic signal, should contain at least three points, as shown in Fig. 13. So another expression of V_{Nm} can

be obtained,

$$V_{N_m} = V_s K(0 - T_0/2)^2 - V_s K(2/f_s - T_0/2)^2 \quad (15)$$

Substituting (14) into (15), the expression of N_m can be achieved, given by

$$N_m = \frac{2k(0 - T_0/2)^2}{k(0 - T_0/2)^2 - k(2/f_s - T_0/2)^2} = \frac{T_0^2 f_s^2}{4(T_0 f_s - 2)} \quad (16)$$

When the time duration T_0 is much larger than $2/f_s$, which is always the case in practice, (16) can be simplified to

$$N_m = \frac{T_0 f_s}{4} \quad (17)$$

From (17), the maximum split number is determined by the time duration of the parabolic signal and the sampling rate of the parabolic signal generator.

Substituting (17) into (13), the maximum achievable TBWP of the generated LFM signal is

$$TBWP_m = \frac{4N_m \gamma_s}{\pi} \approx \frac{T_0 f_s \gamma_s}{\pi} \quad (18)$$

Since the time duration of the generated signal is T_0 , the maximum bandwidth of the generated signal is

$$B_{fm} = \frac{f_s \gamma_s}{\pi} \quad (19)$$

As can be seen from (19), when the modulation index is a constant, the maximum bandwidth is related to the maximum sampling rate of the electrical waveform generator. According to the Nyquist sampling theorem, the maximum bandwidth B_{Em} generated by an electrical waveform generator with a sampling rate of f_s should be less than $f_s/2$. However, in the practical applications, an empirical formula is concluded, which is

$$B_{Em} = \frac{f_s}{2.4} \quad (20)$$

so the proposed method can improve the maximum bandwidth by

$$R_B = \frac{B_{fm}}{B_{Em}} = \frac{2.4\gamma_s}{\pi} \quad (21)$$

With a modulation index larger than $\pi/2.4$, the bandwidth of the generated LFM signal will be larger than that of the LFM signal which is directly generated by the electrical waveform generator.

The maximum time duration is dependent on the sampling rate and the memory depth of the electrical waveform generator, which can be expressed as,

$$T_0 = \frac{M_{fs}}{f_s} \quad (22)$$

where M_{fs} is the number of the maximum memory points of the electrical waveform generator. To generate an LFM signal with a large time duration, one has to increase the sampling point number or decrease the sampling rate.

Substituting (22) into (18), the expression of TBWP becomes

$$TBWP'_m = \frac{T_0 f_s \gamma_s}{\pi} = \frac{M_{fs} \gamma_s}{\pi} \quad (23)$$

It is interesting that the maximum TBWP depends only on the number of the maximum sampling points of the electrical waveform generator when the modulation index of the PoIM is a constant.

In our experiment, the modulation index γ_s is around π , the number of the maximum sampling points M_{fs} is 1.6×10^{10} and the maximum sampling rate f_s is 65 GSa/s. Therefore, the maximum bandwidth of the LFM signal generated based on the proposed method can be as high as 65 GHz, which is 2.4 times of that of the electrical waveform generator (27 GHz). The maximum TBWP can be as high as 1.6×10^{10} . If the half-wave voltage of the PoIM can be decreased and the maximum tolerable power of the PoIM can be increased in the future, γ_s can be enlarged and therefore the TBWP and bandwidth can be further increased.

V. CONCLUSION

A photonic method to generating LFM waveforms with an improved TBWP was proposed and comprehensively studied. By splitting a parabolic signal into N pieces with uniform amplitudes and applying it to an external-phase-modulation based LFM signal generator, the TBWP of the LFM signal can be improved by $N/2$ times. An experiment to verify the feasibility of the proposed scheme was carried out. LFM signals with TBWP improved by more than 500 times are generated. The tunability of the bandwidth and the central frequency are evaluated. The distortions introduced by the non-ideal waveforms and imperfect orthogonally polarization modulation are analyzed. The maximum achievable bandwidth, pulse width and TBWP are theoretically predicted. The system can also work with the RPML to further increase the bandwidth and TBWP. The proposed method is compatible with all the external-phase-modulation based LFM signal generators, which can find applications in modern radar systems.

REFERENCES

- [1] M. I. Skolnik Ed., *Radar Handbook*, 2nd ed. New York, NY, USA: McGraw-Hill, 1991.
- [2] S. L. Pan, D. Zhu, and F. Z. Zhang, "Microwave photonics for modern radar systems," *Trans. Nanjing Univ. Aeronaut. Astronaut.*, vol. 31, no. 3, pp. 219–240, 2014.
- [3] J. D. McKinney, D. E. Leaird, and A. M. Weiner, "Millimeter-wave arbitrary waveform generation with a direct space-to-time pulse shaper," *Opt. Lett.*, vol. 27, no. 15, pp. 1345–1347, 2002.
- [4] A. Krishnan, M. Knapczyk, L. G. de Peralta, A. A. Bernussi, and H. Temkin, "Reconfigurable direct space-to-time pulse-shaper based on arrayed waveguide multiplexers and digital micromirrors," *IEEE Photon. Technol. Lett.*, vol. 17, no. 9, pp. 1959–1961, Sep. 2005.
- [5] C. Wang and J. P. Yao, "Photonic generation of chirped millimeter-wave pulses based on nonlinear frequency-to-time mapping in a nonlinearly chirped fiber Bragg grating," *IEEE Trans. Microw. Theory Techn.*, vol. 56, no. 2, pp. 542–553, Feb. 2008.
- [6] Y. Mei *et al.*, "Photonic generation of chirped microwave signals with high time-bandwidth product," *Opt. Commun.*, vol. 316, pp. 106–110, Apr. 2014.

- [7] J. Ye *et al.*, "Two-dimensionally tunable microwave signal generation based on optical frequency-to-time conversion," *Opt. Lett.*, vol. 35, no. 15, pp. 2606–2608, 2010.
- [8] H. Zhang, W. Zou, and J. Chen, "Generation of a widely tunable linearly chirped microwave waveform based on spectral filtering and unbalanced dispersion," *Opt. Lett.*, vol. 40, no. 6, pp. 1085–1088, 2015.
- [9] A. Rashidinejad and A. M. Weiner, "Photonic radio-frequency arbitrary waveform generation with maximal time-bandwidth product capability," *J. Lightw. Technol.*, vol. 32, no. 20, pp. 3383–3393, Oct. 2014.
- [10] Y. Li, A. Dezfouliyan, and A. M. Weiner, "Photonic synthesis of spread spectrum radio frequency waveforms with arbitrarily long time apertures," *J. Lightw. Technol.*, vol. 32, no. 20, pp. 3580–3587, Oct. 2014.
- [11] H. Jiang *et al.*, "Photonic generation of phase-coded microwave signals with tunable carrier frequency," *Opt. Express*, vol. 38, no. 8, pp. 1361–1363, 2013.
- [12] P. Ghelfi, F. Scotti, F. Laghezza, and A. Bogoni, "Photonic generation of phase-modulated RF signals for pulse compression techniques in coherent radars," *J. Lightw. Technol.*, vol. 30, no. 11, pp. 1638–1644, Jun. 2012.
- [13] W. Li, W. T. Wang, W. H. Sun, L. X. Wang, and N. H. Zhu, "Photonic generation of arbitrarily phase-modulated microwave signals based on a single DDMZM," *Opt. Express*, vol. 22, no. 7, pp. 7446–7457, Apr. 2014.
- [14] W. Li, F. Kong, and J. Yao, "Arbitrary microwave waveform generation based on a tunable optoelectronic oscillator," *J. Lightw. Technol.*, vol. 31, no. 23, pp. 3780–3786, Dec. 2013.
- [15] H. Chi and J. P. Yao, "Photonic generation of phase-coded millimeter-wave signal using a polarization modulator," *IEEE Microw. Wireless Compon. Lett.*, vol. 18, no. 5, pp. 371–373, May 2008.
- [16] Z. Li, M. Li, H. Chi, X. M. Zhang, and J. P. Yao, "Photonic generation of phase-coded millimeter-wave signal with large frequency tunability using a polarization maintaining fiber Bragg grating," *IEEE Microw. Wireless Compon. Lett.*, vol. 21, no. 12, pp. 694–696, Dec. 2011.
- [17] W. Li, N. H. Zhu, and L. X. Wang, "Perfectly orthogonal optical single-sideband signal generation based on stimulated Brillouin scattering," *IEEE Photon. Technol. Lett.*, vol. 24, no. 9, pp. 751–753, May 2012.
- [18] Y. M. Zhang and S. L. Pan, "Generation of phase-coded microwave signals using a polarization-modulator-based photonic microwave phase shifter," *Opt. Lett.*, vol. 38, no. 5, pp. 766–768, Mar. 2013.
- [19] S. F. Liu, D. Zhu, Z. W. Wei, and S. L. Pan, "Photonic generation of widely tunable phase-coded microwave signal based on a dual-parallel polarization modulator," *Opt. Lett.*, vol. 39, no. 13, pp. 3958–3961, Jul. 2014.
- [20] Y. M. Zhang, F. Z. Zhang, and S. L. Pan, "Frequency-doubled and phase-coded RF signal generation based on orthogonally polarized carrier-suppressed double sideband modulation," in *Proc. Asia Commun. Photon. Conf. 2014*, 2014, Paper AF3A.2.
- [21] Y. M. Zhang, F. Z. Zhang, and S. L. Pan, "Frequency-multiplied phase-coded signal generator based on optical polarization division multiplexing Mach-Zehnder modulator," *IEEE Trans. Microw. Theory Techn.*, to be published. doi: 10.1109/TMTT.2016.2616878
- [22] W. Li and J. Yao, "Generation of linearly chirped microwave waveform with an increased time-bandwidth product based on a tunable optoelectronic oscillator and a recirculating phase modulation loop," *J. Lightw. Technol.*, vol. 32, no. 20, pp. 3573–3579, Oct. 2014.
- [23] Y. M. Zhang, X. W. Ye, and S. L. Pan, "Photonic generation of linear frequency-modulated waveform with improved time-bandwidth product," in *Proc. IEEE 2015 Int. Top. Meet. Microw. Photon.*, 2015, Paper WeB.6.
- [24] Y. M. Zhang and S. L. Pan, "Frequency-multiplying microwave photonic phase shifter for independent multichannel phase shifting," *Opt. Lett.*, vol. 41, no. 6, pp. 1261–1264, Mar. 2016.
- [25] S. L. Pan and Y. M. Zhang, "A tunable and wideband microwave photonic phase shifter based on a single sideband polarization modulator and a polarizer," *Opt. Lett.*, vol. 37, no. 21, pp. 4483–4485, Nov. 2012.

Yamei Zhang (S'13) received the B.S. degree, in 2012, from Nanjing University of Aeronautics and Astronautics, Nanjing, China, where she is currently working toward the Ph.D. degree in the Key Laboratory of Radar Imaging and Microwave Photonics and the Ministry of Education.

Her current research focuses on microwave photonic signal generation and processing.

Xingwei Ye (S'14) received the B.S. degree, in 2014, from Nanjing University of Aeronautics and Astronautics, Nanjing, China, where he is currently working toward the Ph.D. degree in the Key Laboratory of Radar Imaging and Microwave Photonics and the Ministry of Education.

His research interests include photonic technologies for signal processing, RF direct sampling, and multibeamforming.

Qingshui Guo received the B.S. degree, in 2015, from Nanjing University of Aeronautics and Astronautics, Nanjing, China, where he is currently working toward the Master's degree in the Key Laboratory of Radar Imaging and Microwave Photonics and the Ministry of Education.

His current research focuses on microwave photonic signal generation.

Fangzheng Zhang received the B.S. degree from Huazhong University of Science and Technology, Wuhan, China, and the Ph.D. degree from Beijing University of Posts and Telecommunications, Beijing, China, in 2008 and 2013, respectively.

He is currently with the Key Laboratory of Radar Imaging and Microwave Photonics and the Ministry of Education, Nanjing University of Aeronautics and Astronautics, Nanjing, China. His research interests include microwave photonics, coherent optical communications, and all-optical signal processing.

Shilong Pan (S'06-M'09-SM'13) received the B.S. and Ph.D. degrees in electronics engineering from Tsinghua University, Beijing, China, in 2004 and 2008, respectively.

From 2008 to 2010, he was a "Vision 2010" Postdoctoral Research Fellow in the Microwave Photonics Research Laboratory, University of Ottawa, Ottawa, ON, Canada. In 2010, he joined the College of Electronic and Information Engineering, Nanjing University of Aeronautics and Astronautics, Nanjing, China, where he is currently a Full Professor and Deputy Director in the Key Laboratory of Radar Imaging and Microwave Photonics and the Ministry of Education. He has authored or coauthored more than 270 research papers, including more than 140 papers in peer-reviewed journals and 130 papers in conference proceedings. His current research focuses on microwave photonics, which includes optical generation and processing of microwave signals, ultrawideband over fiber, photonic microwave measurement, and integrated microwave photonics.

Dr. Pan is a senior member of the IEEE Microwave Theory and Techniques Society, the IEEE Photonics Society, the IEEE Instrumentation and Measurement Society, and a member of the Optical Society of America. He received an OSA Outstanding Reviewer Award in 2015. He is currently a Topical Editor for Chinese Optics Letters. He was a Chair of the numerous international conferences and workshops, including the TPC Chair of the International Conference on Optical Communications and Networks in 2015, the TPC Chair of the high-speed and broadband wireless technologies subcommittee of the IEEE Radio Wireless Symposium in 2013, 2014, and 2016, the TPC Chair of the optical fiber sensors and microwave photonics subcommittee chair of the Optoelectronics and Communication Conference in 2015, a Chair of the microwave photonics for broadband measurement workshop of International Microwave Symposium in 2015, and the TPC Co-Chair of the IEEE MWP 2017.